INSTITUTE OF PHYSICS PUBLISHING COMBUSTION THEORY AND MODELLING

Combust. Theory Modelling **7** (2003) 301–315 PII: S1364-7830(03)36280-1

Numerical modelling of soot formation and oxidation in laminar coflow non-smoking and smoking ethylene diffusion flames

Fengshan Liu[1,3], **Hongsheng Guo**[1], **Gregory J Smallwood**[1] **and Ömer L Gülder**[2]

[1] Combustion Technology Group, Institute for Chemical Process and Environmental Technology, National Research Council, 1200 Montreal Road, Ottawa, Ontario, Canada K1A 0R6
[2] Institute for Aerospace Studies, University of Toronto, 4925 Dufferin Street, Toronto, Ontario, Canada M3H 5T6

E-mail: fengshan.liu@nrc-cnrc.gc.ca

Received 24 April 2002, in final form 13 February 2003
Published 3 April 2003
Online at stacks.iop.org/CTM/7/301

Abstract

A numerical study of soot formation and oxidation in axisymmetric laminar coflow non-smoking and smoking ethylene diffusion flames was conducted using detailed gas-phase chemistry and complex thermal and transport properties. A modified two-equation soot model was employed to describe soot nucleation, growth and oxidation. Interaction between the gas-phase chemistry and soot chemistry was taken into account. Radiation heat transfer by both soot and radiating gases was calculated using the discrete-ordinates method coupled with a statistical narrow-band correlated-k based band model, and was used to evaluate the simple optically thin approximation. The governing equations in fully elliptic form were solved. The current models in the literature describing soot oxidation by O_2 and OH have to be modified in order to predict the smoking flame. The modified soot oxidation model has only moderate effects on the calculation of the non-smoking flame, but dramatically affects the soot oxidation near the flame tip in the smoking flame. Numerical results of temperature, soot volume fraction and primary soot particle size and number density were compared with experimental data in the literature. Relatively good agreement was found between the prediction and the experimental data. The optically thin approximation radiation model significantly underpredicts temperatures in the upper portion of both flames, seriously affecting the soot prediction.

[3] Author to whom correspondence should be addressed.

1364-7830/03/020301+15$30.00

1. Introduction

Development of modelling capabilities for soot formation and oxidation in hydrocarbon flames is of importance for many practical applications. Unfortunately the processes of soot inception, growth and oxidation are very complex and they are not fully understood. Consequently, no universal soot model exists that is equally applicable for different fuels and for different flame conditions. The detailed soot models developed by Frenklach and co-workers [1–3] consider about 600 elementary reactions and 200 species, and such models are currently infeasible for implementation into a multidimensional flame code to predict soot formation. Several semi-empirical soot models have been developed and used to calculate soot in both laminar [4, 5] and turbulent flames [6] with some success.

Modelling of soot formation in a laminar coflow diffusion flame is of greater interest than that in a counterflow flame since it involves all the important physical and chemical processes that affect soot, such as multidimensional flow fields, thermal radiation, finite rate chemistries of gas-phase species and soot. On the other hand, it is simple enough to allow calculations using rather detailed gas-phase chemistry and sophisticated treatment of thermal radiation with tolerable computing time. Almost all the numerical studies of soot formation in laminar diffusion flames reported in the literature were conducted under non-smoking conditions. An exception is the attempt to model a smoking ethylene coflow diffusion flame made by Kennedy *et al* [4] using a semi-empirical two-equation soot model, unfortunately without success. The fact that the two-equation soot model predicts the peak integrated soot volume fraction quite well in the smoking flame implies that the nucleation and surface growth sub-models are relatively effective and the severe drawback is in the soot oxidation model currently employed in the literature. Kennedy *et al* suggested that the failure of the prediction of the smoking flame is attributed to the overprediction of the rate of soot oxidation by O_2 based on the Nagle–Strickland–Constable (NSC) model [7] in the postflame region where the flame temperature is relatively low. The role played by the OH oxidation model in the postflame region, however, was not discussed. While research towards the understanding of soot inception and surface growth is very important, a detailed knowledge of soot oxidation is also crucial to understanding the soot distribution in flames since the amount of soot is the result of these two competing processes. The numerical study of Kennedy *et al* [4] highlights the important role of soot oxidation model in the prediction of smoking flames and a need for the improvement of the current soot oxidation models.

The most important oxidative agents of soot in flames have been identified to be OH, O and O_2 [8–13]. Experimental evidence exists that the NSC model overpredicts the oxidation rate of soot [14] and synthetic chars [15] at temperatures below 1800 K. Although some uncertainty also exists in the soot oxidation model by OH associated with the collision efficiency of OH attack on soot particle and how it varies with temperature [4, 9, 11–13, 16], it seems that there is no direct experimental evidence indicating a similar behaviour of the current OH oxidation model to that of the NSC model at relatively low temperatures. On the other hand, in an experimental study of several coflow smoking flames, Kent and Wagner [17] observed that the burnout cut-off points (an axial location beyond which the area-integrated soot volume fraction is constant implying that soot oxidation essentially ceases) in different smoking flames correlate remarkably well with a soot temperature of around 1300 K based on thermocouple measurement. More recently, Lee and Na [18] found that the burnout cut-off point is about 1400 K based on measurements using two-colour pyrometry in coflow smoking C_2H_4 and C_2H_4/C_3H_8 flames at elevated pressures. The experimental findings of Kent and Wagner [17] and Lee and Na [18] have not been incorporated into existing soot oxidation models. The mechanism of transition from non-smoking to smoking behaviour as the fuel flow rate increases

has been investigated by Glassman and Yaccarino [19] and Kent and Wagner [17]. The earlier study of Glassman and Yaccarino considered the role of oxygen leakage at the nozzle tip as the mechanism of this transition. The study of Kent and Wagner demonstrated that the transition from a non-smoking to a smoking flame is caused by insufficient soot oxidation, due to increased radiation heat transfer resulting in lowered temperatures in the upper portion of the flame.

In this paper, numerical calculations of soot formation and oxidation were conducted in axisymmetric coflow laminar diffusion ethylene flames at atmospheric pressure under both non-smoking and smoking conditions, for which experimental studies have been carried out by Santoro *et al* [20] and Megaridis and Dobbins [21, 22]. Detailed gas-phase chemistry and complex thermal and transport properties of species were used in the calculations. A modified version of the two-equation soot model proposed by Leung *et al* [23] was employed to predict soot nucleation and growth. Use of this simple soot formation model is adequate for the purpose of this paper since the emphasis of this paper is on the soot oxidation models. The objectives of this paper are (i) to propose a phenomenological model of soot oxidation by O_2 and OH based on the existing models in the literature and the experimental studies of Kent and Wagner [17] and Lee and Na [18], (ii) to demonstrate that the smoking flame of Santoro *et al* [20] can be successfully reproduced numerically using the modified soot oxidation model and (iii) to quantitatively evaluate the optically thin approximation (OTA) radiation model against the results based on a more accurate radiation model in the calculations of the two flames.

2. Model formulation and numerical method

The fully elliptic governing equations of mass, momentum, energy and species in axisymmetric cylindrical coordinates (r, z) given in [24] were solved in this paper. The gravitational term was included in the momentum equation in the z-direction. Correction diffusion velocities in both r- and z-directions were used to ensure that the mass fractions of gaseous species and soot sum to unity. The thermophoretic velocities of soot in both the r- and z-directions were accounted for, as were the interactions between the gas-phase chemistry and the soot chemistry.

2.1. Radiation model

The source term in the energy equation due to radiation heat transfer was calculated using the discrete-ordinates method (DOM) in axisymmetric cylindrical geometry described by Truelove [25] along with the T_3 quadrature [26] and the central difference scheme. A statistical narrow-band correlated-k (SNBCK) based band model (bandwidth 250 cm^{-1}) developed by Liu *et al* [27, 28] was employed to obtain the absorption coefficients of CO, CO_2 and H_2O at each band. Based on the experimental measurement of Buckius and Tien [29], the spectral absorption coefficient of soot was assumed to be $5.5 f_v \nu$ with f_v being the soot volume fraction and ν the wavenumber of each spectral band. The integrated radiation intensity at each spectral band was calculated using the 4-point Gauss–Legendre quadrature scheme [30]. The spectrally integrated radiation source term was evaluated by summing up contributions from 36 spectral bands covering the spectral range 150–9150 cm^{-1}. The OTA radiation model is more commonly applied for calculations of laminar coflow diffusion flames, even in sooting flames [4, 5]. To obtain a quantitative comparison with the DOM/SNBCK method, the OTA was also used to calculate the radiation source term in the energy equation with the Planck absorption coefficient of the mixture containing CO, CO_2, H_2O and soot calculated from the same band model used in DOM calculations.

2.2. Soot model

A modified version of the semi-empirical two-equation formulation of soot kinetics [23] was used to model soot nucleation, growth and oxidation. The transport equations for the soot mass fraction and number density are given as

$$\rho v\frac{\partial Y_s}{\partial r}+\rho u\frac{\partial Y_s}{\partial z}=-\frac{1}{r}\frac{\partial}{\partial r}(r\rho V_{T,r}Y_s)-\frac{\partial}{\partial z}(\rho V_{T,z}Y_s)+S_m \tag{1}$$

$$\rho v\frac{\partial N}{\partial r}+\rho u\frac{\partial N}{\partial z}=-\frac{1}{r}\frac{\partial}{\partial r}(r\rho V_{T,r}N)-\frac{\partial}{\partial z}(\rho V_{T,z}N)+S_N \tag{2}$$

where Y_s is the soot mass fraction and N is the soot number density defined as the particle number per unit mass of mixture. Variables u, v, ρ represent velocities in the z- and r-directions and the mixture density. Quantities $V_{T,r}$ and $V_{T,z}$ are the thermophoretic velocities of soot in the r- and z-directions, respectively, and are calculated as

$$V_{T,i}=-0.67\frac{\mu}{\rho T}\frac{\partial T}{\partial x_i},\qquad x_i=r,z \tag{3}$$

The constant in equation (3) is larger than the commonly used value of 0.55 (based on an accommodation coefficient of 0.9 [20]) as a result of a much smaller value of the accommodation coefficient of about 0.3 recently reported by Snelling *et al* [31]. The source term S_m in equation (1) accounts for the contributions of soot nucleation, surface growth and oxidation. The simplified soot nucleation and growth mechanism proposed by Leung *et al* [23] was followed which assumes that acetylene is the only soot nucleation and growth species. Based on the consideration of carbon conservation, the nucleation and surface growth processes are described as [23]

$$C_2H_2\rightarrow 2C(S)+H_2 \tag{R1}$$

$$C_2H_2+nC(S)\rightarrow (n+2)C(S)+H_2 \tag{R2}$$

The rates of nucleation and growth are given as

$$r_1=k_1(T)[C_2H_2]\qquad (\mathrm{kmol\,m^{-3}\,s^{-1}}) \tag{4}$$

$$r_2=k_2(T)f(A_s)[C_2H_2]\qquad (\mathrm{kmol\,m^{-3}\,s^{-1}}) \tag{5}$$

where $f(A_s)$ denotes the functional dependence of soot surface growth on soot surface area per unit volume and $[C_2H_2]$ is the mole concentration of acetylene. It is assumed that the functional dependence is linear, i.e. $f(A_s)=A_s$. The soot surface area per unit volume is calculated as $A_s=\pi(6/\pi)^{2/3}\rho_{C(S)}^{-2/3}Y_s^{2/3}\rho N^{1/3}$ with the density of soot $\rho_{C(S)}$ taken to be $1.9\,\mathrm{g\,cm^{-3}}$ [21, 22]. The kinetic constants in the nucleation and growth rates used in the present calculations are $k_1=1.7\exp(-7548/T)\,(\mathrm{s^{-1}})$ and $k_2=6\exp(-6038/T)\,(\mathrm{m\,s^{-1}})$.

Soot oxidation by OH and O_2 was accounted for in this paper based on the considerations of the uncertainties in the collision efficiencies of O and OH in flames [9–13], i.e. soot oxidation by O radical was not explicitly considered. Reactions of soot oxidation by O_2 and OH are assumed to proceed through

$$0.5O_2+C(S)\rightarrow CO \tag{R3}$$

$$OH+C(S)\rightarrow CO+H \tag{R4}$$

The reaction rates per unit surface area of these two reactions ($\mathrm{kg\,m^{-2}\,s^{-1}}$) are given as

$$r_3=120\left[\frac{k_A X_{O_2}\chi}{1+k_Z X_{O_2}}+k_B X_{O_2}(1-\chi)\right]f_{O_2},\qquad \chi=\left(1+\frac{k_T}{k_B X_{O_2}}\right)^{-1} \tag{6}$$

$$r_4=\varphi_{OH}k_4(T)T^{-1/2}X_{OH}f_{OH} \tag{7}$$

where X_{OH} denotes the mole fraction of OH, and ϕ_{OH} is the collision efficiency for OH attacking on soot particles. The rates of soot oxidation by O_2 and OH are based, respectively, on the NSC model [7] and the Fenimore and Jones model [8] with rate constants for r_3 and r_4 taken from [32]. A constant value of 0.2 is assumed for ϕ_{OH}, which is higher than the experimental value of about 0.1–0.13 [8, 9, 11] to partially compensate the neglect of soot oxidation by the O radical in this paper. The commonly used NSC and OH soot oxidation rates were modified in this paper by introducing two temperature dependent correction factors f_{O_2} and f_{OH} in equations (6) and (7) defined below based on the experimental results of Chan *et al* [14], Levendis *et al* [15], Kent and Wagner [17] and Lee and Na [18]. If f_{OH} is assumed to be the same as f_{O_2}, the amount of emitted soot in the smoking flame is very low compared to the experimental data. Instead, a faster decaying f_{OH} around 1600 K was assumed as defined below. Therefore, two different correction factors were introduced for soot oxidation rates by O_2 and OH. Overall, the correction factors were tuned numerically to match the amount of emitted soot in the smoking flame. The factor f_{O_2} is defined as $f_{O_2} = (1 + \exp[-(T - 1650)/80])^{-1}$, i.e. it is essentially 1 for temperatures above 2000 K, negligibly small for temperatures below about 1300 K as shown in figure 1. The factor f_{OH} is defined as $f_{OH} = (1+\exp[-(T-1675)/70])^{-1}$ for $T \geqslant 1675$ K, $f_{OH} = (1 + \exp[-(T - 1675)/50])^{-1}$ for 1600 K $< T <$ 1675 K and $f_{OH} = 0.1824 \times (1 + \exp[-(T - 1600)/85])^{-1}$ for $T \leqslant 1600$ K. As shown in figure 1, factor f_{OH} is similarly dependent on temperature as f_{O_2} in terms of lower and upper cut-off temperatures. However, f_{OH} decreases more rapidly than f_{O_2} for temperatures between 1600 and 1800 K and then decays slower towards 0. The lower cut-off limit of about 1300–1400 K is based on the experimental work of Lee and Na [18] using two-wavelength pyrometry and the earlier measurement by Kent and Wagner [17] using a thermocouple. Our numerical experiments indicated that the transition from a non-smoking to a smoking flame and the amount of emitted soot are very sensitive to the values of f_{OH} and f_{O_2} at temperatures below about 1650 K, which is a manifestation of the extremely strong coupling between soot radiation and soot oxidation kinetics. The exact physical and chemical processes associated with the modified soot oxidation rates shown in figure 1 are currently not well understood and should be an active research subject in the future.

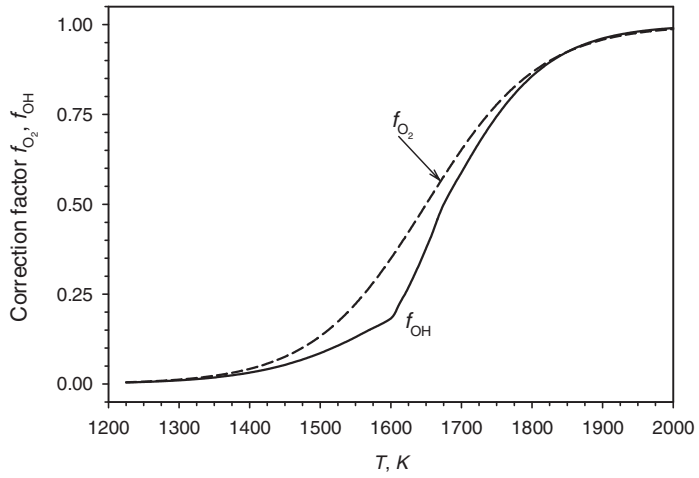

Figure 1. Variation of correction factors f_{O_2} and f_{OH} in the modified soot oxidation model with temperature.

The source term in equation (1), taking into account contributions of soot nucleation, soot surface growth and soot oxidation by O_2 and OH, is therefore written as

$$S_m = 2r_1 M_s + 2r_2 M_s - (r_3 M_s A_s + r_4 A_s) \tag{8}$$

where M_s is the soot molecular weight (12 g mol^{-1}).

The source term in equation (2) represents the production and destruction of the number density of soot particles due to nucleation and agglomeration and is written as [23]

$$S_N = \frac{2}{C_{\min}} N_A r_1 - 2C_a \left(\frac{6M_{C(S)}}{\pi \rho_{C(S)}}\right)^{1/6} \left(\frac{6\kappa T}{\rho_{C(S)}}\right)^{1/2} [C(s)]^{1/6} [\rho N]^{11/6} \tag{9}$$

where N_A is Avogadro's number (6.022×10^{26} particles/kmol), κ is the Boltzman constant (1.38×10^{-23} J K^{-1}), $C_{\min}$ is the number of carbon atoms in the incipient carbon particle (700, which gives a soot inception particle diameter of about 2.4 nm), and C_a is the agglomeration rate constant. The typical values of C_a used in the literature are 3 [33, 34] and 9 [23]. Almost all the current semi-empirical soot models assume that the soot number density decreases as a result of particle agglomeration into spherical aggregates. The only exception is perhaps the study of Ezekoye and Zhang [34] who investigated the effect of particle agglomeration by setting C_a to zero, i.e. neglecting particle agglomeration. It has been established experimentally that soot aggregates consist of more or less identical and point-contact primary soot particles and the primary soot particle number density remains almost constant in the *soot growth region* of a coflow laminar ethylene smoking diffusion flame [21, 22]. It is also well known from both experiments [20, 21] and numerical modelling [5, 35] that the surface growth process is the dominant route for the increase of soot yield. In other words, primary soot particle coalescence (collisional growth to form spherical clusters), which may be significant in the early stage of particle inception, is not important in the surface growth and oxidation stages and can be neglected. These experimental findings suggest that it may be physically reasonable to neglect the destruction term of the soot number density by setting C_a to zero, at least in the soot growth region and further downstream. As a result of this assumption, the number density N represents the number density of primary soot particles. Consequently, the primary soot particle diameter d_p is related to soot mass fraction Y_s and number density N through

$$d_p = \left(\frac{6Y_s}{\pi \rho_{C(S)} N}\right)^{1/3} \tag{10}$$

2.3. Numerical method

The transport equations for mass, momentum, energy, gas-phase species, soot mass fraction, soot number density and radiation intensity are closed with the ideal gas state equation to relate the mixture density to pressure, temperature and mass fractions of gaseous species and appropriate boundary conditions at each side of the computational domain. The governing equations are discretized using the control volume method on a staggered grid. Diffusion terms in the transport equations are discretized by the central difference and the convection terms by the upwind scheme. The SIMPLE algorithm [36] was used to treat the pressure and velocity coupling. Conservation equations of gas-phase species are solved in a fully coupled fashion at each control volume using a direct solver to ensure the convergence process as described by Liu *et al* [37]. All other transport equations are solved using the tridiagonal-matrix algorithm.

3. Results and discussion

The gas-phase reaction mechanism used was basically GRI-Mech 3.0 [38]. The only modification is the removal of all the reactions and species related to NO_x formation. All

the thermal and transport properties were obtained by using the database of GRI-Mech 3.0 and the CHEMKIN codes [39, 40].

The laminar coflow ethylene–air diffusion flames at atmospheric pressure numerically studied here had been previously investigated experimentally [20–22]. The flames were generated with a burner in which pure ethylene flows through an uncooled 11.1 mm inner diameter vertical steel tube and the air flows from the annular region between the fuel tube and a 101.6 mm inner diameter tube. The flow rates and mean velocities of the non-smoking and the smoking flame are the same as those of flame nos 2 and 4, hereafter referred to as F2 and F4, in the experimental study of Santoro *et al* [20]. The mean velocities of the fuel and air streams are 3.98 cm s^{-1} (flow rate 3.85 cm^3 s^{-1}), 8.9 cm s^{-1} (flow rate 713.3 cm^3 s^{-1}) and 5.05 cm s^{-1} (flow rate 4.9 cm^3 s^{-1}), 13.3 cm s^{-1} (flow rate 1068.3 cm^3 s^{-1}) for the non-smoking and the smoking flames, respectively. The inlet temperatures of fuel and air are both 300 K in the calculations. The effect of fuel preheat was not considered in the present calculations. Our previous study [41] indicated that the effect of fuel/burner preheat is primarily in the near burner region and only affects the calculated soot field by about 13%. The inclusion of the preheat effect will improve the predicted temperature in the near burner field, but does not alter the overall results and conclusions obtained in this paper. Unless otherwise indicated, radiation heat transfer was calculated using the DOM coupled with the SNBCK model and the temperature dependent correction factors shown in figure 1 were used in the calculations.

Non-uniform grids were used in both the r- and z-directions to provide greater resolution in the large gradient regions without an excessive increase in the computing time. Very fine grids were placed between 0 and 1.2 cm in the r-direction (resolution less than 0.2 mm) and near the burner exit in the z-direction (less than 0.5 mm up to $z = 12$ cm). Location $z = 0$ corresponds to the burner exit surface. The dimensions of the solution domain and grid size used in all the calculations were respectively 15.35 cm(z) $\times$ 6 cm(r) and 332(z) $\times$ 87(r). Boundary conditions were specified as: axial symmetry along the centreline, free-slip along the $r = 6$ cm boundary and zero-gradient at the $z = 15.35$ cm exit boundary. A parabolic velocity profile was assumed for the fuel stream and a boundary layer type velocity profile for the air stream at the inlet boundary.

It was checked that further refinement of the computational mesh has negligible effect on the results. On the other hand, use of a coarser computational grid results in lower peak soot volume fraction in both flames and significantly less emitted soot in the smoking flame. Overall the calculated results of the smoking flame are more sensitive to the grid resolution than those of the non-smoking flame. Calculations were carried out on a Pentium 4 2.0 GHz PC. Each iteration required about 5 min cpu time and each run required about 1000 iterations to achieve convergence (the maximum relative error of soot volume fraction less than 1.0×10^{-3}).

3.1. Temperature

The predicted radial distributions of temperature in the non-smoking flame at three heights above the burner exit face, $z = 20$, 50 and 70 mm, are compared with the experimental data of Santoro *et al* [20] in figure 2. At $z = 20$ mm, the predicted temperature is significantly lower than the data in the centreline region mainly due to the neglect of the effect of fuel preheat by heat conduction from the flame base to the fuel pipe in the present calculations. At $z = 50$ mm, the predicted temperatures are in good agreement with the experimental data. At $z = 70$ mm, the computed temperatures are significantly higher than the experimental data in the radial range between about $r = 0.2$ and 0.5 cm, which is caused by soot oxidation in this region in the calculation. As shown in figure 5(a), the predicted soot volume fraction distribution always exhibits an annular structure. However, the measured soot volume fraction distribution has an

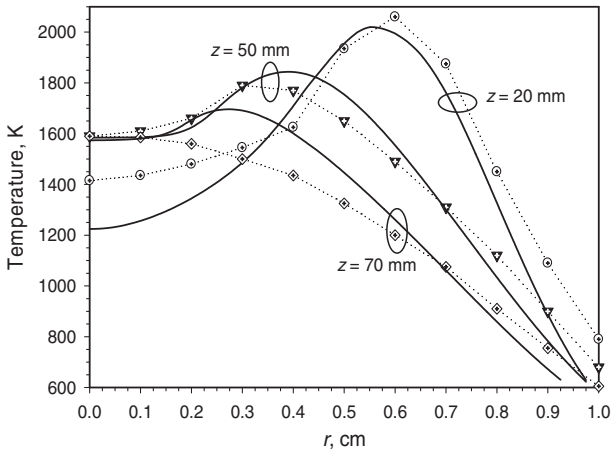

Figure 2. Comparison of the predicted radial temperature distributions at three flame heights in the non-smoking flame with the experimental data of Santoro *et al* [20].

annular structure at low and middle flame heights of F2 and becomes cone-shaped near the flame tip [20]. Overall the predicted temperatures are in reasonably good agreement with the experimental data.

The temperature fields in the non-smoking and smoking flames are compared in figure 3. The peak flame temperatures in F2 and F4 occur, respectively, at $r = 0.55$ cm, $z = 2.13$ cm and $r = 0.6$ cm, $z = 2.18$ cm and the peak temperature in F4 is only about 8 K higher than that in F2. The reason for the similar peak temperatures is that soot concentrations are very low at an axial distance of about 2 cm and therefore radiation heat loss from soot is small. Further downstream, however, the temperatures in F4 in the centreline region are significantly lower due to greater radiation heat loss as not only the soot concentration in F4 is much higher but also F4 emits soot leading to a much larger soot-containing volume, see figure 5. The effect of employing the simple OTA in the calculation of radiation heat transfer on the modelling of F2 and F4 is displayed in figure 4 where the centreline temperatures are shown. Numerical results reveal that use of the OTA only slightly lowers the peak centreline flame temperatures in these two flames. However, the OTA significantly underpredicts the temperatures near the flame tip, especially in the smoking flame, due to neglect of radiation absorption and the strong coupling between temperature and soot oxidation in the upper portion of the flame. Neglect of self-absorption in the OTA predicts a lower flame temperature, which in turn reduces the soot oxidation rate and results in more soot emitted from this flame. The OTA predicts a much higher amount of emitted soot from this flame, see figure 7. The large difference between the two temperature profiles using the two different radiation models in the smoking flame (F4) beyond about 9 cm is precisely caused by the strong coupling between radiation and soot oxidation kinetics, in particular the modified soot oxidation models introduced in this paper through the two correction factors. The large difference between the DOM and OTA temperature profiles in figure 4 and the integrated soot volume fractions shown in figure 7 beyond about 9 cm are, to some extent, a consequence of introducing the two temperature sensitive correction factors in the rates of soot oxidation by O_2 and OH.

3.2. Distribution of soot volume fraction

The predicted soot volume fractions ($f_v = \rho Y_s/\rho_{C(S)}$) in the non-smoking and smoking flames are shown in figure 5. The overall shape of the soot volume fraction distribution is in qualitative

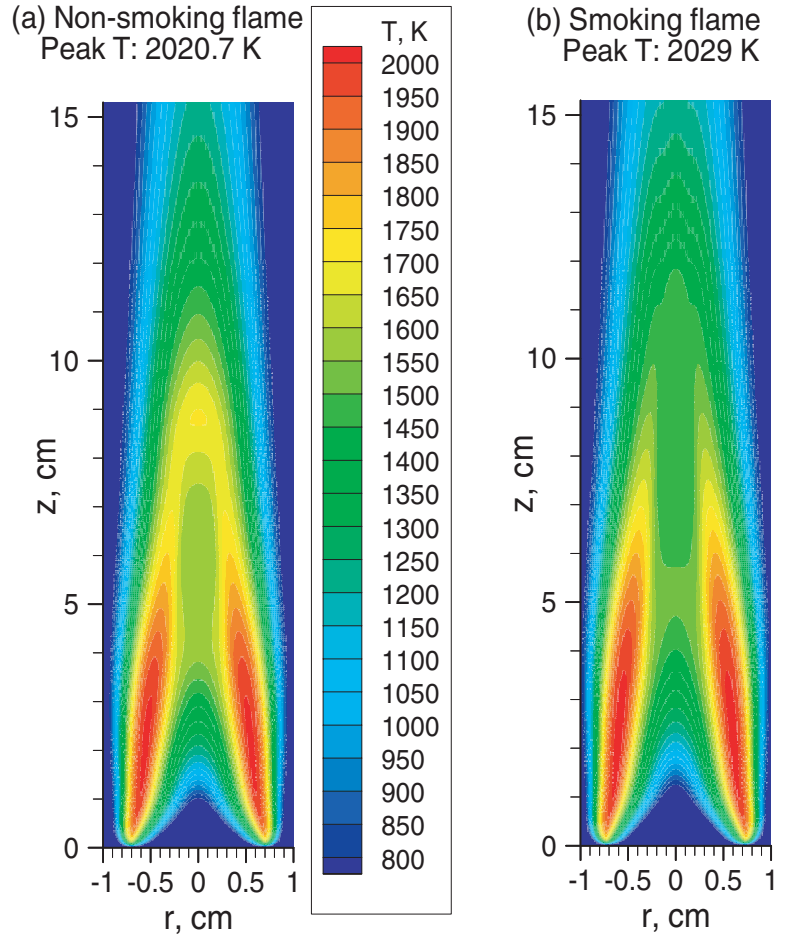

Figure 3. Comparison of the predicted temperature fields in the non-smoking and smoking flames.

agreement with experimental observations. The major drawback of soot models based on the C_2H_2 growth mechanism is that they fail to predict the amount of soot in the centreline region compared to measurements, as also observed previously by Kennedy *et al* [4]. Our numerical experiments indicate that lowering the activation energies in soot nucleation and surface growth rates do not significantly improve the soot volume fractions in the centreline region. The predicted peak soot volume fractions in the non-smoking and the smoking flames are, respectively, 9.9 ppm and 15.9 ppm and are in good agreement with the experimental results of about 9 and 13 ppm of Santoro *et al* [20]. The present soot model with the modified soot oxidation rates by OH and O_2 successfully predicts the transition from non-smoking flame to smoking flame when flow conditions are changed.

3.3. Integrated soot volume fraction

The distribution of the predicted integrated soot volume fraction as a function of the flame height in the non-smoking flame is compared with the experimental data of Santoro *et al* [20] in figure 6. The integrated soot volume fraction is defined as the integration of soot volume

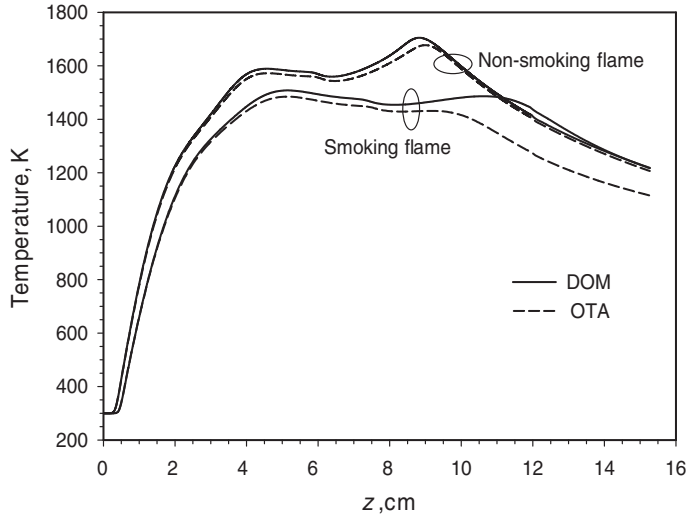

Figure 4. Comparison of the predicted centreline temperature distributions in the non-smoking and the smoking flames using both the DOM/SNBCK and the OTA models.

fraction across the flame (in the radial direction) at a given axial location, i.e. $\int_0^\infty f_v 2\pi r \, dr$ [20]. The predicted values are significantly lower than the experimental data in the lower part of the non-smoking flame (for $z < 3$ cm), which may be primarily due to overestimate of soot concentration in the experiment using the laser intensity attenuation technique since it cannot differentiate soot from PAH, which is likely to be present at these locations. At higher locations, the predicted integrated soot volume fractions are in excellent agreement with the experimental data. It is seen from figure 6 that the predicted visible flame height of about 8.6 cm based on the present soot model is also in excellent agreement with the value of 8.8 cm reported by Santoro *et al* [20]. Use of the OTA radiation model leads to lower integrated soot volume fractions around the location of the peak value, $z = 4$ cm, due to overestimate of radiation heat loss leading to reduced growth rate. Near the flame tip, however, the amount of soot based on the OTA radiation model is greater as a result of reduced soot oxidation rate caused again by excessive heat loss. Use of the OTA radiation model results in a taller visible flame height. The predicted integrated soot volume fractions in this flame are significantly, but not dramatically, affected when the standard soot oxidation models ($f_{O_2} = 1$, $f_{OH} = 1$) are used. Use of the standard oxidation models leads to significant reduction in the amount of soot in the upper portion of the flame and in the visible flame height, as a result of higher rates of oxidation by O_2 and OH.

The predicted integrated soot volume fractions along the flame height in the smoking flame are compared with the experimental data of Santoro [20] in figure 7. Again, the predicted distribution of the integrated soot volume fraction is in overall good agreement with the data, especially the quantity of soot emitted from the open tip of the flame. Use of the OTA results in a much higher amount of soot emitted, caused by reduced soot oxidation rates due to excessive heat loss in the upper portion of the flame as shown in figure 4. The relative importance of separately modifying the rates of oxidation by O_2 and OH is also illustrated in figure 7. While the modification of the oxidation rate by OH is shown to be more critical than that by O_2, these results demonstrate that it is necessary to modify the rates of soot oxidation by both O_2 and OH in order to numerically predict the transition from a non-smoking flame to a smoking

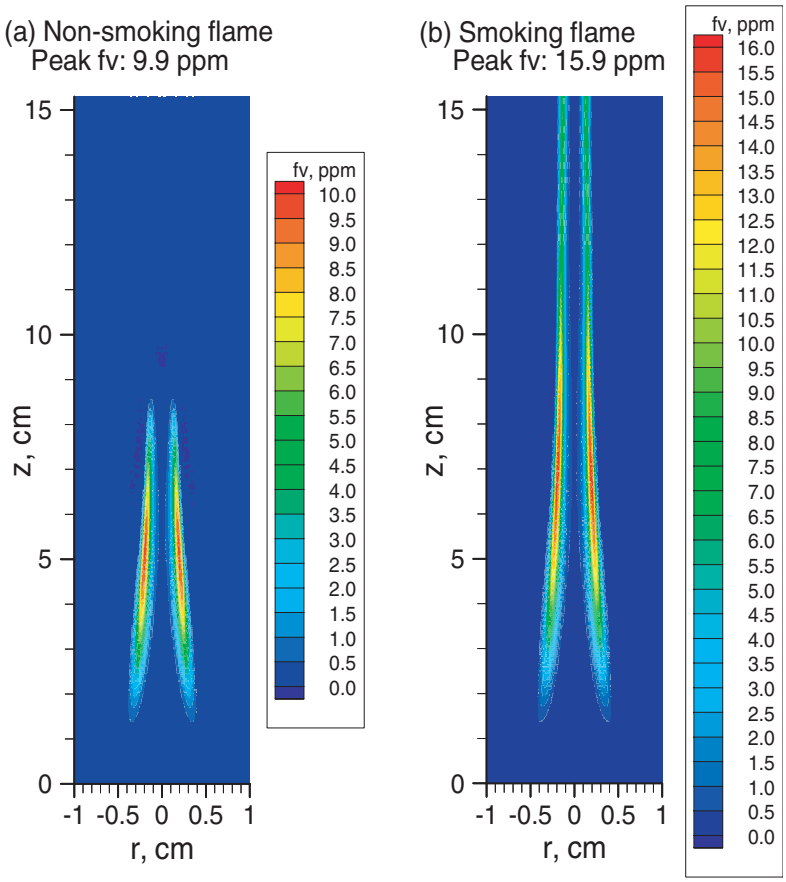

Figure 5. Comparison of the predicted soot volume fraction distributions in the non-smoking and the smoking flames.

flame when the fuel flow rate increases, as well as the correct amount of soot emitted in the smoking flame.

3.4. Primary soot particle size and number density

The predicted primary soot particle number density and primary soot particle diameter along the annular region of maximum soot volume fraction in both the non-smoking flame and the smoking flame are compared with the experimental data of Megaridis and Dobbins [21, 22] in figures 8 and 9, respectively. The experimental data of Megaridis and Dobbins [21, 22] show that the values of primary soot particle number density in both flames are similar in most of the soot growth region, suggesting that the nucleation rates in these flames are of similar strength. Indeed, numerical results indicate that the peak nucleation rate in F4 is only about 3% higher than that in F2. Numerical results are in good qualitative and reasonable quantitative agreement with the experimental data in both flames. The numerical results show that the number densities along the path exhibiting maximum soot volume fraction in the two flames are very close to each other in the lower portion of the growth region, $z < 4$ cm, and increase almost linearly with the distance from the burner exit surface. Further downstream, the predicted number density

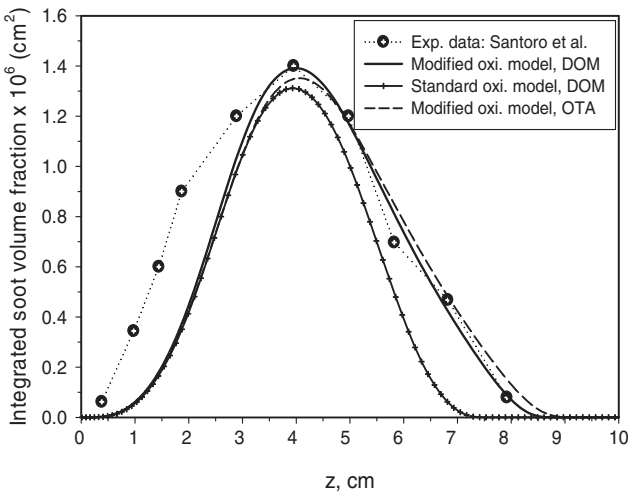

Figure 6. Comparison of the integrated soot volume fraction along the flame height in the non-smoking flame. Numerical results based on the standard oxidation model ($f_{O_2} = 1$, $f_{OH} = 1$) and the OTA radiation model are also plotted. The experimental data are from Santoro *et al* [20].

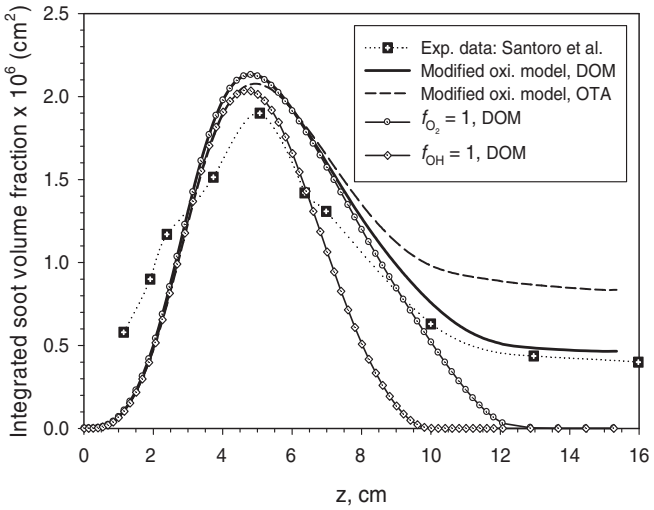

Figure 7. Comparison of the integrated soot volume fraction along the flame height in the smoking flame. Effects of using the OTA radiation model and the relative importance of modification of the O_2 and OH oxidation rates on the prediction are also shown. The experimental data are from Santoro *et al* [20].

along the path of maximum soot in the smoking flame continues to increase but at a slower rate. In contrast, the particle numerical density along the path of maximum soot in the non-smoking flame reaches its peak at about $z = 6.5$ cm then decreases. It should be pointed out that the decrease in the primary soot particle number density along the path of maximum soot in the non-smoking flame is not a consequence of destruction, since neither particle coalescence nor soot oxidation was taken into account as a destruction mechanism of the soot particle number density in the present calculations. A careful examination of the numerical results reveals that

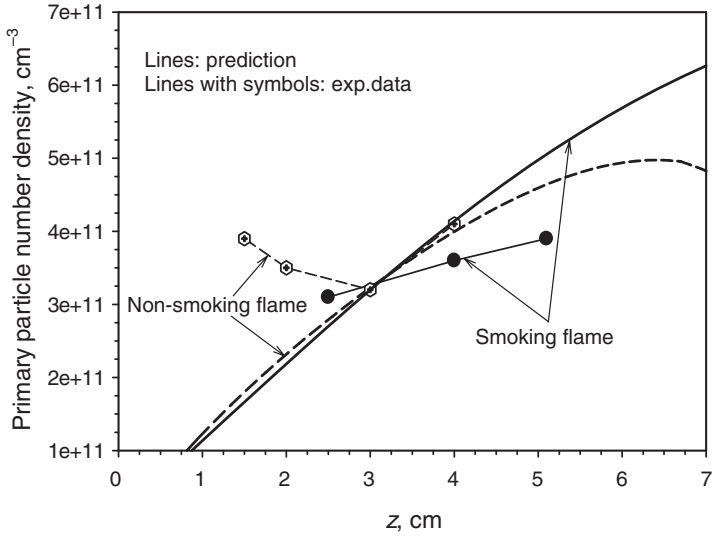

Figure 8. Comparison of the predicted and measured primary soot particle number density along the annular region exhibiting maximum soot volume fraction in the non-smoking and the smoking flame. The experimental data are from Megaridis and Dobbins [21, 22].

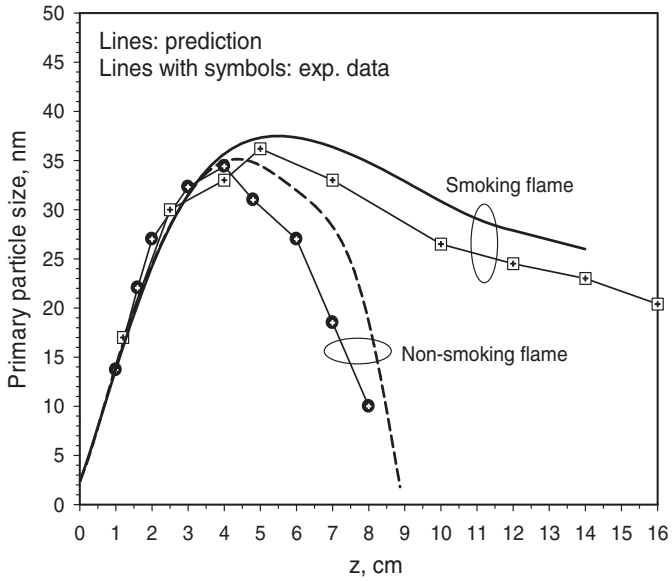

Figure 9. Comparison of the predicted and measured primary soot particle diameter along the annular region exhibiting maximum soot volume fraction in the non-smoking and the smoking flame. The experimental data are from Megaridis and Dobbins [22].

the path of maximum soot volume fraction and the path of maximum soot particle number density start to deviate from each other in the upper portion of the flame in F2. However, the path of maximum soot volume fraction and the path of maximum soot particle number density coincide through the flame in F4.

Although the present soot model somewhat overpredicts the primary soot particle size in the upper part of both flames ($z > 4$ cm), the quantitative agreement between the prediction and the experimental data is considered quite good in both flames. This is actually expected based on the relatively good agreement between the calculated and measured soot volume fractions shown in figures 6 and 7 and primary soot particle number densities shown in figure 8, since d_p is derived from soot concentration and number density using equation (10). It is interesting to observe that the model successfully reproduces the almost identical primary soot particle sizes in the lower part of these two flames ($z < 4$ cm), implying that the soot surface growth rates in these two flames are very similar. Numerical results show that the peak soot growth rate in F4 is only about 20% higher than that in F2. Beyond about $z = 4$ cm, primary particle sizes continue to increase at lower rates, due to reduced growth rate and increased oxidation rate, and eventually start to decrease.

4. Conclusions

A numerical study of soot formation and oxidation in coflow ethylene diffusion flames under both non-smoking and smoking conditions was conducted using detailed gas-phase chemistry and a modified two-equation soot model. An improved model for soot oxidation by O_2 and OH was suggested based on available experiments. The improved soot model is capable of reproducing the characteristics of soot including the peak soot volume fraction, the integrated soot volume fraction, the primary soot particle size and number density in both the non-smoking and the smoking flame. Numerical results indicate that it is important to accurately calculate radiation heat transfer in the two flames investigated, especially in the smoking flame. It is also necessary to modify *both* the existing O_2 oxidation model and the OH oxidation model in order to correctly predict the amount of soot emitted from the smoking flame. It is evident that further experimental research is required to study soot oxidation by O_2, OH and O at temperatures below 1800 K. The improved soot oxidation model needs to be evaluated by direct experimental evidence and comparison in other smoking flames.

References

[1] Frenklach M, Clary D W, Gardiner W C Jr and Stein S E 1984 *Proc. Combust. Inst.* **20** 887–901
[2] Frenklach M and Wang H 1990 *Proc. Combust. Inst*. **23** 1559–66
[3] Frenklach M and Wang H 1994 Detailed mechanism and modeling of soot particle formation *Soot Formation in Combustion: Mechanism and Models* ed H Bockhorn (*Springer Series in Chemical Physics vol 59*) (Berlin: Springer) pp 162–90
[4] Kennedy I M, Yam C, Rapp D C and Santoro R J 1996 *Combust. Flame* **107** 368–82
[5] Smooke M D, McEnally C S, Pfefferle L D, Hall R J and Colket M B 1999 *Combust. Flame* **117** 117–39
[6] Brookes S J and Moss J B 1999 *Combust. Flame* **116** 486–503
[7] Nagle J and Strickland-Constable R A 1962 Oxidation of carbon between 1000–2000°C *Proc. 5th Conf. on Carbon* (London: Pergamon) pp 154–64
[8] Fenimore C P and Jones G W 1967 *J. Phys. Chem*. **71** 593–7
[9] Neoh K G, Howard J B and Sarofim A F 1981 Soot oxidation in flames *Particulate Carbon: Formation During Combustion* ed D C Siegla and G W Smith (New York: Plenum) pp 261–77
[10] Bradley D, Dixon-Lewis G, El-Din Habik S and Mushi E M J 1984 *Proc. Combust. Inst*. **20** 931–40
[11] Garo A, Prado G and Lahaye J 1990 *Combust. Flame* **79** 226–33
[12] Roth P, Brandt O and Von Gersum S 1990 *Proc. Combust. Inst*. **23** 1485–91
[13] Puri R, Santoro R J and Smyth K C 1994 *Combust. Flame* **97** 125–44
[14] Chan M L, Moody K N, Mullins J R and Williams A 1987 *Fuel* **66** 1694–8
[15] Levendis Y A, Flagan R C and Gavalas G R 1989 *Combust. Flame* **76** 221–41
[16] Haudiquert M, Cessou A, Stepowski D and Coppalle A 1997 *Combust. Flame* **111** 338–49
[17] Kent J H and Wagner H Gg 1984 *Combust. Sci. Technol*. **41** 245–69

[18] Lee W and Na Y D 2000 *JSME Int. J.* B **43** 550–5
[19] Glassman I and Yaccarino P 1981 *Proc. Combust. Inst.* **18** 1175–83
[20] Santoro R J, Yeh T T, Horvath J J and Semerjian H G 1987 *Combust. Sci. Technol.* **53** 89–115
[21] Megaridis C M and Dobbins R A 1988 *Proc. Combust. Inst.* **22** 353–62
[22] Megaridis C M and Dobbins R A 1989 *Combust. Sci. Technol.* **66** 1–16
[23] Leung K M, Lindstedt R P and Jones W P 1991 *Combust. Flame* **87** 289–305
[24] Kuo K K 1986 *Principles of Combustion* (New York: Wiley) pp 172–205
[25] Truelove J S 1978 AERE-R-9100, AERE, Harwell, UK
[26] Thurgood C P, Becker H A and Pollard A 1995 *J. Heat Transfer* **117** 1068–70
[27] Liu F, Smallwood G J and Gülder Ö L 1999 *AIAA Paper* 99-3679
[28] Liu F, Smallwood G J and Gülder Ö L 2000 *J. Thermophys. Heat Transfer* **14** 278–81
[29] Buckius R O and Tien C L 1977 *Int. J. Heat Mass Transfer* **20** 93–106
[30] Liu F, Smallwood G J and Gülder Ö L 2000 *Int. J. Heat Mass Transfer* **43** 3119–35
[31] Snelling D R, Smallwood G J, Sawchuk R A, Neill W S, Gareau D, Clavel D, Chippior W L, Liu F and Gülder Ö L 2000 *SAE Paper* 2000-01-1994
[32] Moss J B, Stewart C D and Young K J 1995 *Combust. Flame* **101** 491–500
[33] Fairweather M, Jones W P and Lindstedt R P 1992 *Combust. Flame* **89** 45–63
[34] Ezekoye O A and Zhang Z 1997 *Combust. Flame* **110** 127–39
[35] Kaplan C R and Kailasanath K 2001 *Combust. Flame* **124** 275–94
[36] Patankar S V 1980 *Numerical Heat Transfer and Fluid Flow* (New York: Hemisphere)
[37] Liu Z, Liao C, Liu C and McCormick S 1995 *AIAA Paper* 95-0205
[38] Smith G P *et al* http://www.me.berkeley.edu/gri_mech/
[39] Kee R J, Miller J A and Jefferson T H 1980 *Sandia Report* SAND 80-8003
[40] Kee R J, Warnatz J and Miller J A 1983 *Sandia Report* SAND 83-8209
[41] Guo H, Liu F, Smallwood G J and Gülder Ö L 2002 *Combust. Theory Modelling* **6** 173–87